Journal of Quality Measurement and Analysis *JQMA* 22(SI) 2026, 233-250
e-ISSN: 2600-8602 *http://www.ukm.my/jqma*
https://doi.org/10.17576/jqma.22si.2026.13

PATTERN RECOGNITION OF ELECTROMYOGRAPHY SIGNAL IN UPPER LIMB MOVEMENT USING SUPERVISED MACHINE LEARNING: IPSILATERAL HAIR COMBING ACTIVITY

(Pengecaman Corak Isyarat Elektromiografi dalam Pergerakan Anggota Pinggiran Atas Badan Menggunakan Pembelajaran Mesin Diselia: Aktiviti Sikat Rambut Ipsilateral)

ABU BAKAR YAHYA, AZMIN SHAM RAMBELY*, HASYATUN CHE-NAN
& NORUL ELYA SHAHIRA MD SANUSI

ABSTRACT

Surface electromyography (sEMG) provides valuable insights into muscle activation and force generation, especially in tasks involving upper limb movement. However, identifying distinct signal patterns that reliably represent muscular force remains a significant challenge due to variability in physiological signals and motion complexity. This study aims to investigate the relationship between EMG signal features and muscle force exertion during a functional arm movement, specifically, ipsilateral hair combing (IHC) activity, among healthy subjects. EMG data were acquired from deltoid, biceps brachii and palmaris longus during IHC activity. There were 16 healthy participants (male: 5; female: 11; average age: 39.1 years; weight: 72.9 kg; height: 160.7 cm) performed IHC activity while EMG signals were recorded using the EMG data acquisition system (Delsys Bagnoli-8). IHC activity were recorded using the motion capture system (Vicon-Nexus 1.8.1). Four time-domain features such as mean absolute value (MAV), root mean square (RMS), variance (VAR) and maximum amplitude (MAX) were extracted and used as input for classification. Four supervised machine learning models such as Naïve Bayes (NB), Support Vector Machine (SVM), Random Forest (RF) and k-Nearest Neighbors (k-NN) were applied. Model performance was evaluated using confusion matrix, accuracy and F1 score. The pattern recognition framework involved four stages: signal acquisition, feature extraction, model training and testing. The analysis demonstrated a clear correlation between changes in EMG signals and the corresponding muscular force exerted during arm movement phases. Among the classifiers, SVM achieved the highest recognition accuracy which is 83.5% and F1 score of 0.817, indicating its superior capability in distinguishing muscle activation patterns. This study establishes a promising approach for muscle force classification using EMG signals during upper limb movement specifically in IHC activity. The results offer practical implications for assistive rehabilitation systems, especially in monitoring and supporting patients recovering from neurological injuries.

Keywords: electromyography (EMG); features extraction; rehabilitation monitoring; support vector machine (SVM); time domain

ABSTRAK

Elektromiografi (sEMG) memberikan maklumat yang bernilai berkaitan pengaktifan otot dan penjanaan daya, khususnya dalam tugasan yang melibatkan pergerakan anggota atas badan. Walau bagaimanapun, pengecaman corak isyarat yang jelas dan konsisten bagi mewakili daya otot masih merupakan satu cabaran utama disebabkan oleh variasi isyarat fisiologi dan kerumitan pergerakan. Kajian ini bertujuan untuk menyiasat hubungan antara ciri-ciri isyarat EMG dan daya otot yang dikenakan semasa pergerakan fungsi lengan, iaitu aktiviti sikat rambut ipsilateral (SRI), dalam kalangan subjek sihat. Data EMG diperoleh daripada otot deltoid, biceps brachii dan palmaris longus semasa aktiviti SRI dijalankan. Seramai 16 orang peserta sihat (lelaki: 5; perempuan: 11; purata umur: 39.1 tahun; berat badan: 72.9 kg; ketinggian: 160.7 cm) telah melakukan aktiviti SRI, manakala isyarat EMG direkodkan menggunakan sistem pemerolehan data EMG (Delsys Bagnoli-8). Aktiviti SRI turut dirakam menggunakan sistem rakaman pergerakan (Vicon-Nexus 1.8.1). Ciri-ciri domain masa, iaitu nilai mutlak purata, punca min kuasa dua serta varians, diekstrak dan digunakan sebagai input untuk proses pengelasan. Empat model pembelajaran mesin diselia diaplikasi, iaitu Naïve Bayes (NB), Mesin Vektor Sokongan (MVS), Hutan Rawak (HR) dan Jiran Terdekat-k (JT-k). Prestasi model dinilai menggunakan matriks kekeliruan, ketepatan dan skor F1. Rangka kerja pengecaman corak melibatkan empat peringkat utama, iaitu pemerolehan isyarat, pengekstrakan ciri, latihan model dan pengujian. Analisis kajian menunjukkan terdapat hubungan yang jelas antara perubahan isyarat EMG dan daya otot yang dikenakan semasa fasa pergerakan lengan. Antara model pengelas yang digunakan, model MVS mencapai ketepatan pengecaman tertinggi dengan nilai ketepatan dan skor F1, masing-masing adalah 83.5% dan 0.817, yang menunjukkan keupayaan MVS dalam membezakan corak pengaktifan otot. Kajian ini membuktikan satu pendekatan yang berpotensi untuk pengelasan daya otot menggunakan isyarat EMG semasa pergerakan anggota pinggiran atas badan, khususnya dalam aktiviti SRI. Dapatan kajian ini mempunyai implikasi praktikal dalam pembangunan sistem bantuan rehabilitasi, terutamanya bagi pemantauan dan sokongan pesakit yang sedang pulih dari kecederaan neurologi.

Kata kunci: elektromiografi (EMG); pengekstrakan ciri; pemantauan rehabilitasi; mesin vektor sokongan (MVS); domain masa

1. Introduction

Functional arm movement is a complex interplay of neuromuscular coordination and biomechanical control. Understanding this interplay is crucial in clinical rehabilitation, assistive technologies, and motor function assessment. Surface electromyography (sEMG) offers a non-invasive window into this process by capturing the electrical activity generated by muscle contractions. These signals, when appropriately processed and interpreted, provide meaningful representations of muscular force and movement dynamics. It has been widely adopted in studies involving stroke rehabilitation, prosthetics, and motor learning (Tsai *et al.* 2014; Zhang *et al.* 2025).

Despite the advantages of sEMG, mapping raw signals to meaningful representations of muscle force and movement remains a substantial challenge. Factors such as inter-subject variability, signal noise, and task complexity contribute to the difficulty of developing accurate models. Moreover, reliance on a single time-domain feature often fails to capture the full richness of muscular activity, necessitating the use of multi-feature extraction and data-driven modeling approaches. Recent research has shown the application of machine learning to decode EMG signal patterns and classify motor tasks with increasing accuracy. Techniques such as Support Vector Machines (SVM), Random Forests (RF) and deep learning architectures have been successfully applied to classify hand gestures, estimate joint torque and segment movement phases in real time (Halilaj *et al.* 2018). However, studies focusing specifically on functional tasks of daily living activities, such as ipsilateral hair combing (IHC) activity, dressing or reaching object, remain relatively limited, especially when it comes to combining both EMG and motion capture systems for high-fidelity analysis.

This study addresses this gap by investigating the relationship between EMG signal characteristics and muscular force exertion towards arm movement phases during ipsilateral hair combing activity among healthy individuals. Time-domain features were extracted from the recorded EMG signals and used to train supervised machine learning models for pattern recognition. Using supervised machine learning approaches, we aim to identify meaningful EMG patterns corresponding to distinct arm movement phases and evaluate classifier performance using accuracy, F1 score and confusion matrices. The findings are expected to contribute to the development of intelligent rehabilitation systems for early detection and monitoring of upper limb dysfunction in stroke survivors or individuals with neurological impairments.

2. Methods and Materials

2.1. *Subjects*

The participants consisted of 16 healthy adults comprising both male (5) and female (11) individuals with no history of musculoskeletal or neurological disorders. All participants were right-handed to ensure consistency in movement patterns, with mean age 39.1 years (SD± 10.3, range of 24 – 56 years old), mean weight 72.9 kg (SD± 16.5, range of 51.5 - 102.0 kg) and mean height 160.7 cm (SD± 10.2, range of 148 – 185 cm). Prior to participation, each subject provided written informed consent and the experimental protocol was approved by Jabatan Etika Penyelidikan Hospital Universiti Kebangsaan Malaysia (NN-2016-045).

2.2. *Data acquisition and experimental procedures*

To investigate the muscle activation patterns during functional upper limb movement, a hybrid setup combining sEMG and motion capture was employed. EMG signals were collected using commercially available data acquisition system (Delsys Bagnoli-8; Delsys, Boston, MA), a widely validated tool for neuromuscular signal acquisition. Three primary muscles on the dominant side, namely the deltoid, biceps brachii, and palmaris longus, were selected based on their involvement in shoulder flexion, elbow flexion, and wrist positioning, respectively. Electrodes placement followed the Surface Electromyography for the Non-Invasive Assessment of Muscles (SENIAM) guidelines to ensure optimal signal quality and to minimize signal cross-talk (Hermens *et al.* 2000).

In parallel, a motion capture system (Vicon-Nexus 1.8.1; Oxford Metrics Ltd., Oxford, England) was used to track joint movements and synchronize kinematic data with EMG signals, enabling precise segmentation of movement phases. The system used three infrared cameras, with different height positions, to detect 14 reflective markers (six spherical 9 mm and eight spherical 14 mm) placed on the bony landmarks of subject's upper limb. Markers have been placed in the following positions: iliac crest, acromion, mid-humerus, olecranon of the ulna, in the middle of the ulna, styloid process of radial and ulna, the lateral border of the distal and proximal of first, second and fifth metacarpal (Che-Nan & Rambely 2022).

From the pilot study, it was confirmed that the experimental protocol did not interfere with the participants' natural upper limb movement during the IHC activity. In the experiment, each subject was instructed to perform the activity in three consecutive times at a self-selected and comfortable speed. Participants were seated on a 45 cm-high banquet chair with their back supported against the chair backrest to minimise trunk motion throughout the experiment. To ensure familiarity with the task and consistency in performance, subjects practiced the movement five times, and the second, third, and fourth trials were selected for subsequent analysis. This selection helped eliminate potential variability due to initial unfamiliarity or fatigue in later repetitions. All participants performed the task using their dominant hand, which is right hand. The experimental setup is illustrated in Figure 1 and Figure 2. The chosen task and protocol were developed in consultation with clinical professionals and guided by prior literature to ensure relevance to functional daily activities and clinical rehabilitation scenarios. (Hermens *et al*. 2000; Che-Nan & Rambely 2022).

The IHC activity was segmented into five distinct movement phases to facilitate detailed analysis as illustrated in Figure 2. Phase 1 (Initiation or Reaching Phase) began with the subject seated in the standard starting position, with the dominant hand resting on the ipsilateral thigh and the palm facing downward. The hand then reached out to grasp the comb from the table. Phase 2 (Forward Transport) involved lifting and moving the comb toward the right side of the head in preparation for combing. Phase 3 (Combing Execution) was defined as the active combing phase, where the hand performed the combing motion along the length of the hair. Phase 4 (Backward Transport) referred to the movement of returning the comb from the head to the table, followed by releasing it. Finally, Phase 5 (Return to Rest) involved the hand returning to its original resting position on the thigh, completing the full cycle of the task. This movement sequence reflects common daily activities that involve similar upper limb mechanics, such as brushing teeth or reaching for items on shelves.

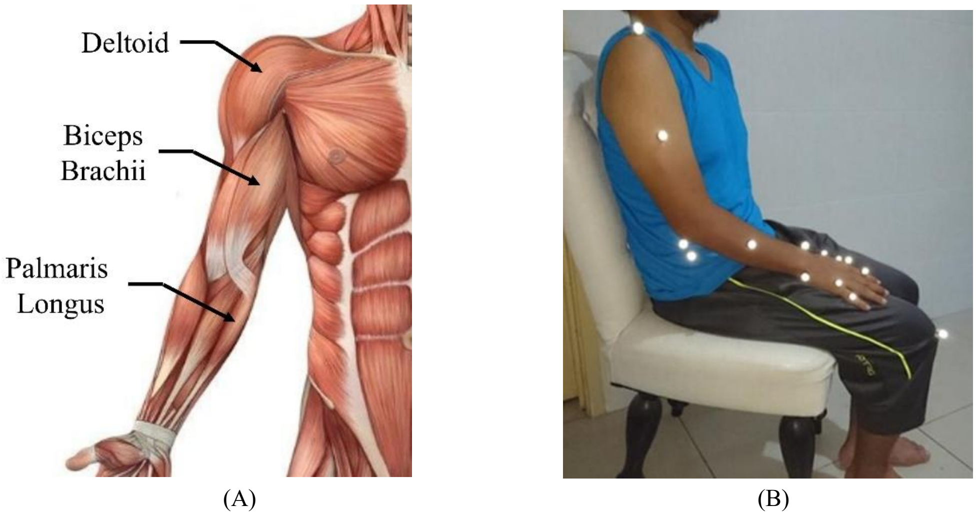

Figure 1: (A) The muscles location for electrodes placement; (B) The markers placement for IHC activity

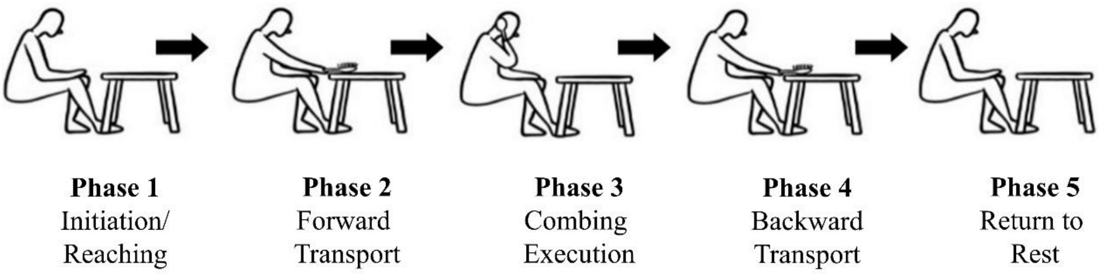

Figure 2: The experimental setup and arm movement phases for IHC activity

2.3. *Data processing and analysis*

EMG data were continuously recorded throughout the task duration. Raw EMG signals were first processed using a band-pass filter with a frequency range of 20 to 450 Hz to remove motion artifacts and a notch filter at 50 Hz to eliminate power line interference. Segmentation was carried out to isolate the active movement phase. Subsequently, four time-domain features, which are mean absolute value (MAV), root mean square (RMS), variance (VAR) and maximum amplitude (MAX), were extracted from each window of the segmented signals. These features were chosen due to their sensitivity to signal amplitude and their proven effectiveness in representing muscle contraction levels (Mohd Khairuddin *et al*. 2021).

The extracted features were then used as input to train four different supervised machine learning models, which are Naïve Bayes (NB), Support Vector Machine (SVM), Random Forest (RF) and k-Nearest Neighbors (k-NN). These algorithms were selected due to their suitability for handling nonlinear EMG data, low-to-moderate feature dimensionality and the presence of signal variability and noise commonly observed in physiological measurements. A k-fold cross-validation strategy was applied to split the dataset into training and testing subsets to ensure generalization and minimize overfitting, using an 80:20 train-test ratio.

2.3.1. Naïve Bayes (NB)

NB is a probabilistic classifier based on Bayes' theorem, which assumes conditional independence among predictors. This classifier estimates the probability that a given EMG feature vector belongs to each movement class and assigns the class with the highest posterior probability. The conditional probability formulation is given by

$$P(y|x_{1,}\ldots,x_n) = \frac{(P_y)P(x_{1,}\ldots,x_n|y)}{P(x_{1,}\ldots,x_n)} \quad , \tag{1}$$

where $P(y|x_{1,}\ldots,x_n)$ represents the conditional probability of a class variable given the input feature vector x, where y denotes the class label and x denotes the input feature vector. $P(y|x_{1,}\ldots,x_n)$ calculates the probability that the given hypothesis is true based on the observed data.

NB assumes conditional independence among EMG features given the class label. Although this assumption does not fully reflect the correlated nature of EMG features, the classifier remains effective for small feature sets and offers high computational efficiency. In this study, class-conditional probability parameters were estimated from the training data and subsequently applied to classify unseen EMG samples.

2.3.2. Support Vector Machine (SVM)

SVM was employed in this study to construct an optimal decision boundary for discriminating between different movement phases based on EMG feature distributions. The SVM classifier was trained using labeled feature vectors with the objective of maximizing the separation between classes.

Conceptually, SVM seeks to identify a separating hyperplane that divides data points from different classes while maximizing the margin between them. A larger margin indicates a more robust separation and reduces the sensitivity of the classifier to noise and variability inherent in EMG signals.

The decision function of SVM can be expressed in a simplified form as:

$$f(x) = sign(w^T x + b) \ , \tag{2}$$

where x denotes the EMG feature vector, w represents the learned weight parameters, and b is the bias term.

As EMG feature distributions are generally nonlinearly separable, a radial basis function (RBF) kernel was applied to map the input data into a higher-dimensional feature space, thereby enabling effective class separation.

2.3.3. Random Forest (RF)

RF was implemented as an ensemble learning approach that combines multiple decision trees to improve classification accuracy and stability. Each decision tree was constructed using a randomly selected subset of training samples and EMG features, introducing diversity among the individual learners.

Within each decision tree, classification decisions are made based on a series of threshold-based rules applied to EMG features such as RMS and MAV. However, the predictive capability of a single decision tree is limited and prone to overfitting.

To address this limitation, RF aggregates the predictions of all decision trees through a majority voting mechanism. The final class prediction can be mathematically expressed as:

$$\hat{y} = \arg max_c \sum_{t=1}^{T} I(h_t(x) = c) \, , \tag{3}$$

where $h_t(x)$ denotes the class prediction of the t-th decision tree for the input vector x, T represents the total number of trees in the forest and forest and $I(\cdot)$ is an indicator function that returns a value of 1 if the condition $(h_t(x) = c)$ is satisfied and 0 otherwise. The variable c corresponds to the candidate class labels associated with the EMG movement phases.

This ensemble strategy enhances robustness against noise and variability in EMG signals and is well suited for nonlinear classification tasks.

2.3.4. k-Nearest Neighbour (k-NN)

The k-NN algorithm classifies an unknown sample based on the majority class among its k nearest neighbors in the feature space. The Euclidean distance is calculated as:

$$d(x, y) = \sqrt{\sum_{i=1}^{n} (x_i - y_i)^2} \quad , \tag{4}$$

where d represents Euclidean distance, x and y are points with n features.

This non-parametric method effectively captures local feature similarities in EMG data. Although k-NN is intuitive and straightforward to implement, its performance is highly dependent on appropriate feature scaling and is sensitive to noise in EMG measurements.

Performance evaluation of the classification models was conducted using several standard metrics, namely the confusion matrix, overall accuracy and F1 score. The confusion matrix provided insights into classification errors and class-level performance, while accuracy measured the proportion of correct predictions across all classes. The F1 score represents the harmonic mean of precision and recall. Unlike overall accuracy, which considers all predictions equally, the F1 score places greater emphasis on correctly identifying true positive cases. It is particularly useful in evaluating the performance of supervised machine learning classifiers, especially when the goal is to balance the trade-off between precision and recall in imbalanced or task-specific datasets. All computational analyses were performed using Python 3.13.5 environments with relevant signal processing and machine learning libraries.

The arm movement data were continuously recorded throughout the task duration. After the recording process was completed, each marker was identified and the movement data were captured using the Vicon-Nexus system, which aims to ensure that each marker is detected properly during the data capture process. In some recordings, markers were sometimes hidden or overlapped with other markers and could be detected automatically. In each analysis, a minimum of three recordings were used for analysis of every subject. From three successful recordings, the mean was calculated as a measurement for each subject. For this activity, data movement was divided into five phases accordingly for the IHC activity. The goal was to gather kinematic data to determine parameters such as angles and velocities of shoulder, elbow and wrist joints for the IHC activity.

3. Results and Discussion

The IHC activity is considered a complex activity from a kinematic perspective. It involves fine motor skills that require a sequence of coordinated movements across distinct phases, incorporating finger manipulation to grasp and control an object—in this case, a hair comb. Functionally, IHC activity is categorized as a basic upper limb movement performed primarily in the sagittal plane while manipulating an external object. This study specifically focuses on the involvement of the shoulder, elbow and wrist joints, which are key contributors to the task. Analysis of the IHC activity is widely utilized in clinical contexts as an assessment tool to highlight the importance of specific motion parameters in activities of daily living (ADL). Several quantitative measures are employed to assess distinctive characteristics of upper limb motion. In this study, the IHC activity is analyzed in terms of movement phases and interjoint coordination, providing a comprehensive framework for evaluating human motor performance. This analysis can be used to assess the effectiveness of rehabilitation interventions, measure upper limb function and yield insights into the fundamental nature and characteristics of human hand movement.

3.1. *Muscle Activation and Joint Kinematics Across IHC Activity Phases*

The IHC activity was segmented into five functional phases to facilitate EMG and kinematic analysis as shown in Figure 3. Each phase was characterized by distinct joint movements which are particularly at the shoulder, elbow and wrist joint; and corresponding patterns of muscle activation. Three primary muscles were analyzed, which are deltoid, biceps brachii and palmaris longus. These muscles represent key contributors to shoulder flexion, elbow movement and wrist or finger control, respectively. A summary of the muscle activation and joint kinematics across IHC activity phases is given in Table 1.

In Phase 1 (Initiation or Reaching Phase), the subject began in an anatomical seated position with the dominant arm resting on the ipsilateral thigh. The movement involved reaching forward in the sagittal plane to grasp a comb placed on the table. During this phase, shoulder flexion increased from approximately 10°–30° at rest to 35°–45° as the arm moved forward. Elbow angles ranged from 70°–110°, progressing to 100°, where 120° as the subject extended the forearm to reach the comb; this angle represented the maximum elbow extension observed during the entire task. Concurrently, the wrist moved into flexion as the fingers prepared to grasp the object. This phase was associated with moderate activation of the deltoid and biceps brachii, reflecting the need for controlled flexion at both shoulder and elbow joints. The palmaris longus showed low activation, as fine motor manipulation was just beginning.

Phase 2 (Forward Transport) began once the comb was firmly grasped. The hand was lifted and brought toward the right side of the head. Kinematic analysis showed that shoulder angles increased further, reaching maximum flexion and abduction between 40°–65°, while the elbow flexed into a 40°–70° range. The wrist maintained flexion to support grip stability. As such, the anterior deltoid exhibited high activation, playing a primary role in lifting and stabilizing the arm. The biceps brachii remained moderately to highly active, particularly in maintaining elbow positioning and forearm control. The palmaris longus showed moderate activation, assisting in object stabilization during arm movement.

In Phase 3 (Combing Execution), the combing motion began once the hand reached the head. At this stage, shoulder and elbow angles remained relatively stable, indicating a quasi-isometric posture. The shoulder was maintained in maximum elevation, while the elbow and wrist worked together to guide the comb through the hair. As the motion required fine wrist and finger control, palmaris longus activation increased substantially. In contrast, both deltoid and biceps brachii displayed moderate to low activity, primarily serving to stabilize limb positioning during the fine motor phase.

Phase 4 (Backward Transport) followed the completion of the combing motion. The arm returned the comb to the table, transitioning from the elevated position back toward the lap. Shoulder flexion decreased to 20°–40° and elbow angles increased again to 90°–120°, representing another maximum elbow extension range during release. The wrist shifted into extension to facilitate object release. This phase involved moderate activation of both the deltoid and biceps brachii, as these muscles controlled arm descent and ensured smooth movement. The palmaris longus also remained moderately active, especially during grip release.

Finally, Phase 5 (Return to Rest) concluded the task cycle. The hand returned to the original anatomical position on the thigh. The shoulder extended back to 5°–30°, and the elbow returned to a flexed position between 100°–120°. The wrist continued into extension to assist in re-positioning the hand comfortably. Muscle activity across all three muscles was minimal, indicating a return to a resting state. This phase served as the motor reset point before subsequent repetitions.

Throughout all phases, the integration of EMG and kinematic data provided valuable insight into the coordination and control strategies employed during a common yet functionally rich daily activity. The distinct activation profiles observed in each phase reinforce the importance of combining biomechanical and electrophysiological analysis for a comprehensive understanding of upper limb function in healthy individuals and potentially in populations undergoing rehabilitation.

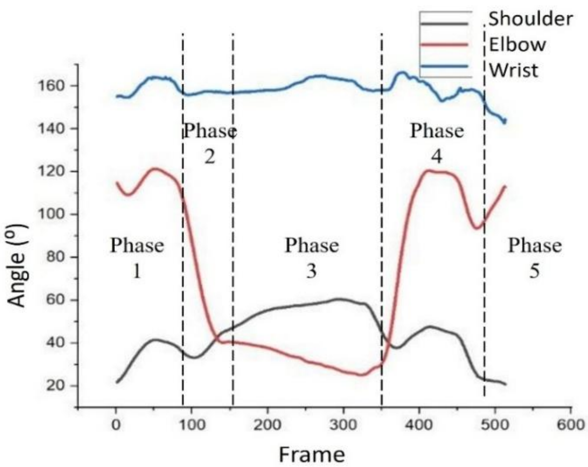

Figure 3: Angle of shoulder, elbow and wrist joints during IHC activity

Table 1: Summary of muscle activation and joint kinematics across IHC activity phases

Phase	Phase Name	Shoulder Angle (°)	Elbow Angle (°)	Wrist Motion	Deltoid (Anterior)	Biceps Brachii	Palmaris Longus	Muscle Function Description
Phase 1	Initiation (Reaching)	10°–30° to 35°–45° (Flexion)	70°–110° to 100°–120° (Extension)	Flexion	Moderate	Moderate	Low	Shoulder and elbow move to reach forward; wrist flexes to grasp comb placed on the table.
Phase 2	Forward Transport	35°–45° to 40°–65° (Abduction)	100°–120° to 40°–70° (Flexion)	Flexion	High	Moderate–High	Moderate	Comb lifted and moved toward the head; shoulder reaches max flexion/abduction; grip maintained during movement.
Phase 3	Combing Execution	Maintained at 40°–65°	Stable around 40°–70°	Fine wrist motion	Moderate–Low	Low–Moderate	High	Fine wrist and finger motion for combing; minimal joint angle changes; wrist in controlled motion.
Phase 4	Backward Transport	40°–65° to 20°–40° (Flexion)	40°–70° to 90°–120° (Extension)	Extension	Moderate	Moderate	Moderate	Arm returns comb to table; grip released; shoulder and elbow extend; wrist extends to drop comb.
Phase 5	Return to Rest	20°–40° to 5°–30° (Extension)	90°–120° to 100°–120° (Flexion)	Extension	Low	Low	Low	Minimal activation as hand returns to initial anatomical position; muscles resume baseline tone.

3.2. *Phase-by-phase EMG characteristics analysis during IHC activity*

The visual inspection of EMG signals plotted separately as shown in Figure 4, for the deltoid, palmaris longus and biceps brachii muscles across the five movement phases revealed distinct activation profiles that correspond closely to the functional demands of each phase in the IHC activity. This individualized approach to signal visualization facilitates a more granular understanding of muscle engagement and control strategy during dynamic upper limb movement.

In the Phase 1 (Initiation or Reaching Phase), the deltoid muscle demonstrated a progressive increase in activation as the arm moved forward from the resting position to reach the comb on the table. The EMG waveform indicated a clear rising trend in amplitude, with several burst-like activations suggesting neuromuscular preparation and recruitment for shoulder flexion. This pattern was supported by concurrent activation in the biceps brachii, reflecting its role in stabilizing elbow flexion during the reach. The palmaris longus also showed early engagement with moderate signal amplitude, corresponding to the wrist flexion required for grasping the comb. These findings are in line with earlier studies that highlight anticipatory proximal muscle activity during goal-directed reach-to-grasp actions (Akbaş *et al.* 2024).

During the Phase 2 (Forward Transport), the deltoid muscle reached its peak activation, as indicated by higher EMG amplitudes with consistent bursts. This corresponds with the shoulder abduction and elevation required to lift the arm toward the head. The biceps brachii showed reduced activity compared to the Phase 1 (Initiation or Reaching Phase), reflecting a minor role in vertical transport, while the palmaris longus maintained steady activation, consistent with ongoing wrist stabilization. The sharp signal peaks in the deltoid during this phase are indicative of increased motor unit recruitment in upward reaching tasks.

In the Phase 3 (Combing Execution), the palmaris longus became the dominant contributor, as reflected in a relatively stable but elevated EMG amplitude. The deltoid maintained moderate activation, likely to support arm positioning, while the biceps brachii showed minimal engagement. The consistent nature of the palmaris signal implies controlled, repetitive wrist movement necessary for combing. This distal muscle control with minimal proximal fluctuation is characteristic of fine motor manipulation, consistent with reports by Steinhart *et al.* (2021), who demonstrated distal stabilization in grooming-related tasks.

The Phase 4 (Backward Transport) was characterized by a secondary rise in deltoid activation as the arm returned the comb to the table. Unlike the initial transport, this phase exhibited slightly more variability in the deltoid signal, possibly reflecting minor postural adjustments during descent. The biceps brachii showed moderate reactivation, particularly in the early portion of the phase, supporting elbow control during the lowering motion. The palmaris longus signal remained consistent, likely assisting with grip release and hand positioning. This pattern suggests a return to more coordinated multi-joint control for cyclical upper limb actions.

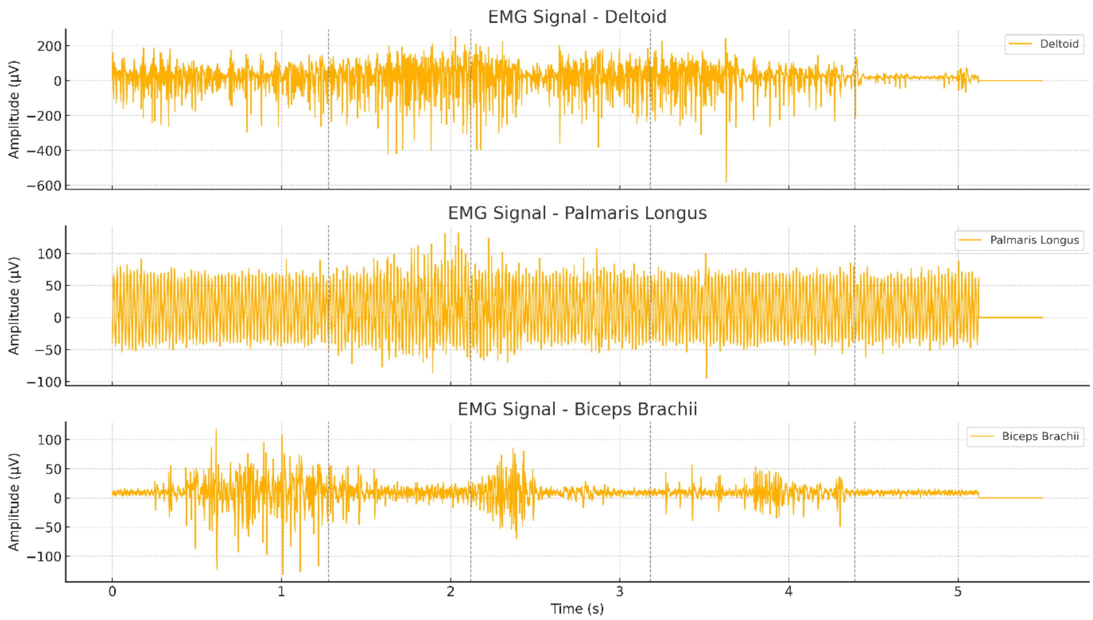

Figure 4: Raw EMG signal at deltoid, palmaris longus and biceps brachii muscles

Finally, the Phase 5 (Return to Rest) showed a significant reduction in EMG amplitude across all three muscles. The deltoid and biceps brachii returned to near-baseline levels, indicating relaxation of proximal segments. The palmaris longus exhibited brief low-amplitude activations, potentially related to minor wrist repositioning. This phase represents a neuromuscular reset, which is muscle deactivation upon task completion in functionally structured upper limb assessments.

Overall, the individualized plots across movement phases offer a comprehensive view of how each muscle behaves during specific segments of a real-world functional task. The EMG patterns observed validate the functional segmentation approach and reinforce the relevance of time-domain features in quantifying muscle contribution. These results serve as a benchmark for future studies involving impaired populations, where deviations from these normative patterns can be used as diagnostic or therapeutic indicators.

3.3. *Relationship EMG signal and arm movement*

The synchronized visualization of the biceps brachii sEMG signal and joint angle trajectories across the IHC activity reveals coordinated neuromuscular strategies that support task-specific biomechanical demands as shown in Figure 5. The EMG waveform demonstrates temporally aligned activation bursts that correspond with key kinematic transitions in shoulder, elbow and wrist joints motion. These findings reflect the muscle's multifaceted role in controlling both gross and fine upper limb movements.

During the Phase 1 (Initiation or Reaching Phase), a gradual increase in biceps brachii activity is evident, corresponding with progressive flexion at the elbow joint and slight forward motion of the shoulder. The angular change in the elbow joint from approximately 70° to over 100°, observed concurrently with a rising EMG envelope, suggests that the biceps acts as a primary mover in initiating forearm lift and stabilization. This is supported by prior work from Mischi and Cardinale (2009), who reported a direct temporal correlation between elbow flexion demands and increased biceps EMG amplitude in reaching tasks. The wrist joint shows minimal angular displacement during this phase, reinforcing the proximal dominance of muscular effort.

In the Phase 2 (Forward Transport), EMG amplitude remains elevated but shows less variability, while elbow angles decrease moderately and shoulder angles peak near their maximum. The biceps appears to contribute both as a stabilizer and as a co-activator to manage dynamic inter-joint coordination. This phase marks a functional transition from power generation to joint stabilization, where biceps activity modulated to support efficient shoulder-elbow coordination.

During the Phase 3 (Combing Execution), the EMG signal plateaus at a moderate level despite minimal angular change in all joints. This suggests that the biceps is not involved in producing movement but rather in maintaining postural tone and resisting gravitational pull during the repetitive combing motion. In the Phase 4 (Backward Transport), a second burst of EMG activity occurs alongside re-extension of the elbow and slight shoulder descent. This renewed activation likely supports the deceleration of the forearm and the controlled return of the comb to the table. Notably, the elbow exhibits its largest angular shift during this phase, from approximately 50° to over 110°, reinforcing the mechanical contribution of the biceps during eccentric control. Similar neuromechanical coupling was reported by Sabzevari *et al.* (2017), who highlighted increased EMG variance during downward transport in bimanual manipulation.

The Phase 5 (Return to Rest) shows a sharp decline in EMG amplitude, coinciding with a return of the elbow angle to baseline and reduced movement at the shoulder and wrist. The transient spikes near the end of the phase may indicate fine-tuning actions during restabilization. These signals, although brief, suggest continued but minimal neuromuscular monitoring of limb position, in line with the proprioceptive role of the biceps observed in fine adjustment tasks.

The synchronized representation of EMG and kinematic data in this study offers a comprehensive view of the functional roles of the biceps brachii across different movement demands. From prime mover during elbow flexion to stabilizer during task maintenance and eccentric controller during return motion, the muscle demonstrates high task-dependence in activation strategy. This nuanced behavior affirms prior claims that muscle activation is contextually modulated not only by joint angle but also by phase-specific movement intention (Schmidt *et al.* 2023).

From an application standpoint, this integrative analysis holds important implications for intelligent rehabilitation systems and assistive device programming. By identifying phase-specific muscle activation profiles and linking them with joint behavior, rehabilitation programs can be tailored to restore functional synergies in patients with neuromotor deficits, such as stroke or spinal cord injury. In particular, EMG-triggered exoskeletons or feedback systems could benefit from phase-aware algorithms that anticipate the type and level of assistance needed in each segment of a daily functional task. The results also support the development of wearable monitoring systems where phase-based EMG patterns are used as digital biomarkers of recovery progression.

In conclusion, the integration of surface EMG and joint angle data offers a multidimensional understanding of neuromuscular control in functional upper limb activities. The findings from the biceps brachii analysis emphasize the importance of temporally and biomechanically synchronized data in characterizing phase-specific muscle function. This approach is essential for advancing precision rehabilitation technologies and promoting motor recovery that is contextually and functionally relevant.

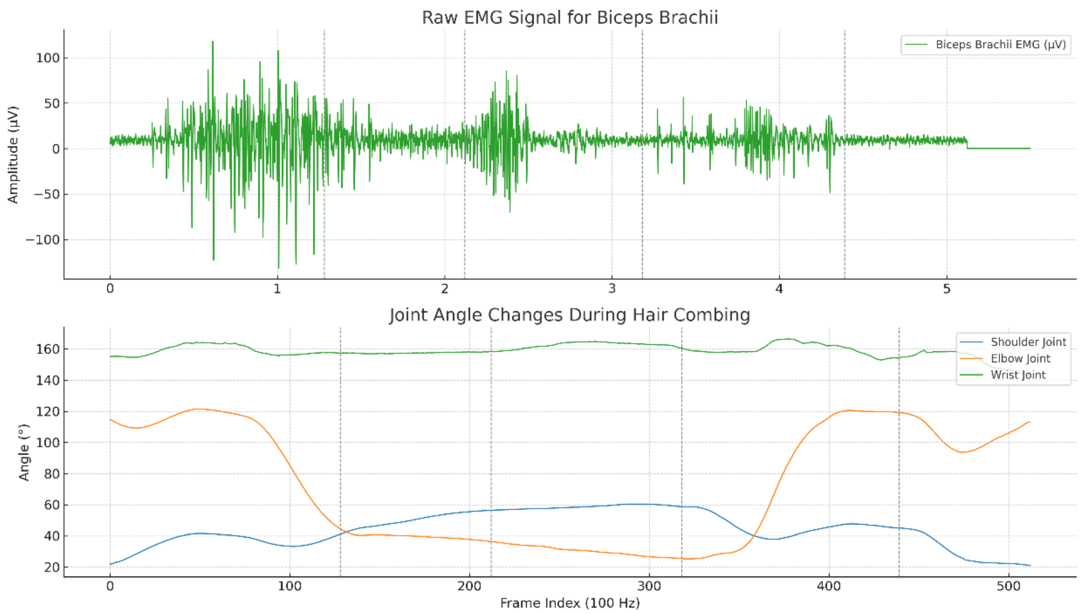

Figure 5: Raw EMG signal of the biceps brachii during the IHC activity (top) and the corresponding joint angle changes for the shoulder, elbow and wrist (bottom). Dased vertical lines indicate the transition points between movement phases

3.4. *EMG signal features extraction analysis*

The analysis of muscle activation patterns across the five defined movement phases of the IHC activity revealed distinct activation signatures in all three muscles studied, which are deltoid, biceps brachii and palmaris longus, corresponding closely to the biomechanical demands of each phase as shown in Table 1 above (section 3.1) and Table 2 below. These findings are consistent with the functional roles of each muscle in upper limb kinematics and support prior research that highlights the sensitivity of time-domain EMG features in reflecting dynamic muscle effort.

During the Phase 1 (Initiation or Reaching Phase), elevated activation was observed in the deltoid and biceps brachii, as evidenced by high RMS and MAV values. This corresponds with the reaching and grasping motion that demands shoulder flexion and elbow stabilization. The palmaris longus showed moderate activation, associated with wrist flexion necessary for grasping the comb. The Phase 2 (Forward Transport) showed a peak in deltoid RMS and maximum amplitude, reflecting increased shoulder abduction and load bearing as the arm moves toward the head. This pattern parallels observations from Yamazaki *et al.* (2003), who reported maximal deltoid and biceps co-activation in arm elevation movements.

The Phase 3 (Combing Execution) was marked by sustained deltoid and palmaris activation with minimal variation in elbow joint angle and relatively stable EMG features, suggesting isometric-like control during repetitive wrist-level motion. Interestingly, the biceps brachii demonstrated reduced activity in this phase, indicating its minor role in the fine motor pattern of combing. These results correspond with Steinhart *et al.* (2021), who noted that distal muscles exhibit higher signal stability during grooming-like tasks, whereas proximal muscles engage primarily during gross transport.

In the Phase 4 (Backward Transport), deltoid and triceps brachii involvement was reflected in the increased deltoid maximum amplitude, likely due to the shoulder extension required to return the arm. The biceps maintained moderate activity, while palmaris longus continued to exhibit consistent amplitude, emphasizing its stabilizing role in hand posture. The Phase 5 (Return to Rest) was characterized by a marked reduction in all EMG features, indicating a return to baseline muscle tone, with only mild wrist extensor and biceps engagement to control limb deceleration. This pattern further confirms the coordination of proximal and distal muscles in terminating upper limb tasks.

The integration of muscle activation profiles with joint angle mapping not only strengthens the biomechanical interpretation but also provides a physiologically grounded reference for clinical modeling of upper limb tasks. The clear phase-specific differences in amplitude and signal variability among muscles provide a foundation for developing adaptive rehabilitation protocols, particularly for stroke patients with impaired motor control. This study's use of four time-domain features, which are MAV, RMS, maximum amplitude and VAR, offers a computationally efficient yet sensitive approach for implementing such systems in mobile or home-based therapy environments.

The significance of these findings lies in their potential application in intelligent rehabilitation systems, where muscle activity data can be used to assess patient compliance, fatigue and motor strategy adaptation over time. Furthermore, the ability to classify and analyze movement phases allows therapists to tailor interventions that target specific muscle groups and kinematic deficiencies. Such systems could be embedded into feedback-rich virtual rehabilitation platforms or physical robotics interfaces for neurorehabilitation.

Future research should therefore involve a larger and more diverse subject pool, including clinical populations such as post-stroke individuals, to validate and extend the model. Incorporating additional EMG features, such as frequency-domain or wavelet-based parameters, could further enhance classification robustness. Real-time implementation and feedback testing in functional rehabilitation contexts would also provide critical insight into system usability and clinical efficacy. Lastly, long-term tracking of EMG evolution during rehabilitation could enable predictive modeling of recovery trajectories, aligning with the broader vision of personalized, data-driven neurotherapy.

Table 2: EMG signal features extraction analysis for deltoid, biceps brachii and palmaris longus muscles during the IHC activity

Phase	Deltoid				Biceps Brachii			
	Max (μV)	RMS (μV)	MAV (μV)	VAR (μV²)	Max (μV)	RMS (μV)	MAV (μV)	VAR (μV²)
Initiation	294.39	67.0	52.42	4172.62	131.51	28.99	21.3	756.41
Forward Transport	420.85	96.51	76.42	9011.23	55.34	14.39	11.63	126.3
Combing Execution	395.27	83.28	64.63	6621.93	85.46	17.43	13.37	222.67
Backward Transport	581.47	74.61	56.38	5259.61	56.47	14.12	11.7	118.83
Return to Rest	113.95	23.47	19.29	301.13	16.16	8.83	8.11	12.11

Phase	Palmaris Longus			
	Max (μV)	RMS (μV)	MAV (μV)	VAR (μV²)
Initiation	90.64	40.43	35.1	1428.15
Forward Transport	131.93	43.49	36.71	1682.65
Combing Execution	123.67	41.16	35.49	1485.73
Backward Transport	99.87	40.98	35.56	1471.58
Return to Rest	88.05	37.3	30.87	1220.95

3.5. *EMG signal classification analysis*

The comparative performance of the classification models used in this study, which are NB, SVM, RF and k-NN, is summarized in Table 3. The table reveals distinct variations in model performance based on F1 scores and overall accuracy, highlighting both the discriminative capacity and reliability of each algorithm when applied to multi-phase upper limb movement classification using EMG signals.

The confusion matrix for the SVM machine learning model is shown in Figure 6. It demonstrates the correct classifications were concentrated along the diagonal, with 27, 38, 27, 33 and 41 correctly identified samples for Phases 1 (Initiation), 2 (Forward), 3 (Combing), 4 (Backward) and 5 (Return), respectively. The highest true positive counts were observed in Phase 2 and Phase 5, indicating strong recognition of these movement segments. Minor misclassifications occurred primarily between neighboring phases, such as Phase 1 misclassified as Phase 2 (n=2) and Phase 3 misclassified as Phase 4 (n=5), which may be attributed to transitional overlaps in EMG signal patterns.

Among the models tested, SVM exhibited the highest classification accuracy (83.5%) and F1 score of 0.817, indicating a strong balance between precision and recall across all movement phases. This aligns with findings by Cai *et al.* (2019), who demonstrated that SVM models generally outperform other classifiers in EMG signal classification due to their effectiveness in handling high-dimensional and non-linear datasets. Similarly, Tepe and Demir (2022) observed that SVM delivered superior performance in classifying complex upper limb gestures in real-time prosthetic control, suggesting its suitability for rehabilitation and assistive technologies. The SVM model's superior margin-based decision-making mechanism likely contributed to its generalization performance, particularly in tasks involving overlapping EMG signal features from adjacent movement phases.

The NB classifier showed a competitive performance with F1 score of 0.769 and accuracy of 77.5%. Despite its simplifying assumption of feature independence, NB remains effective in domains like biomedical signal processing where strong class separation exists. Its low computational cost also supports its use in embedded systems or portable wearable devices, making it a practical choice when real-time feedback with minimal resource consumption is prioritized.

RF model, with F1 score of 0.758 and accuracy of 76.6%, performed comparably to NB but slightly lower than SVM. Its ensemble nature makes it resilient to overfitting and allows it to capture non-linear interactions between EMG features. Studies by Shilaskar *et al.* (2024) highlighted RF's utility in EMG pattern recognition, particularly when used with large, diverse datasets. However, in this context, the overlapping signal characteristics and limited sample size may have constrained the model's ability to effectively isolate phase-specific signal structures.

The k-NN algorithm yielded the lowest performance metrics in this study, with F1 score of 0.685 and classification accuracy of 70.0%. While k-NN is known for its simplicity and non-parametric nature, its performance often deteriorates in noisy or high-dimensional feature spaces, especially when the number of classes is large or class boundaries are not well-defined. This finding is consistent with previous literature, such as the work by Kok *et al.* (2024), which indicated k-NN's susceptibility to local signal variation and class imbalance in EMG-based gesture recognition.

The implications of these findings are significant for the development of intelligent assistive technologies and clinical rehabilitation systems. The consistent performance of the SVM model suggests that it is well-suited for deployment in systems requiring accurate phase detection, such as EMG-controlled prosthetics, robotic exoskeletons, and movement tracking tools for stroke rehabilitation. Nonetheless, there are several limitations inherent to this study. This study used only three EMG channels and time-domain features, which may constrain the models' ability to fully capture inter-muscular coordination and temporal dynamics. Future work should consider integrating frequency-domain and time-frequency-domain features, multi-modal sensor fusion and larger, more diverse datasets. Longitudinal studies evaluating inter-session stability and cross-subject generalizability would also provide deeper insights into the clinical readiness of these machine learning pipelines.

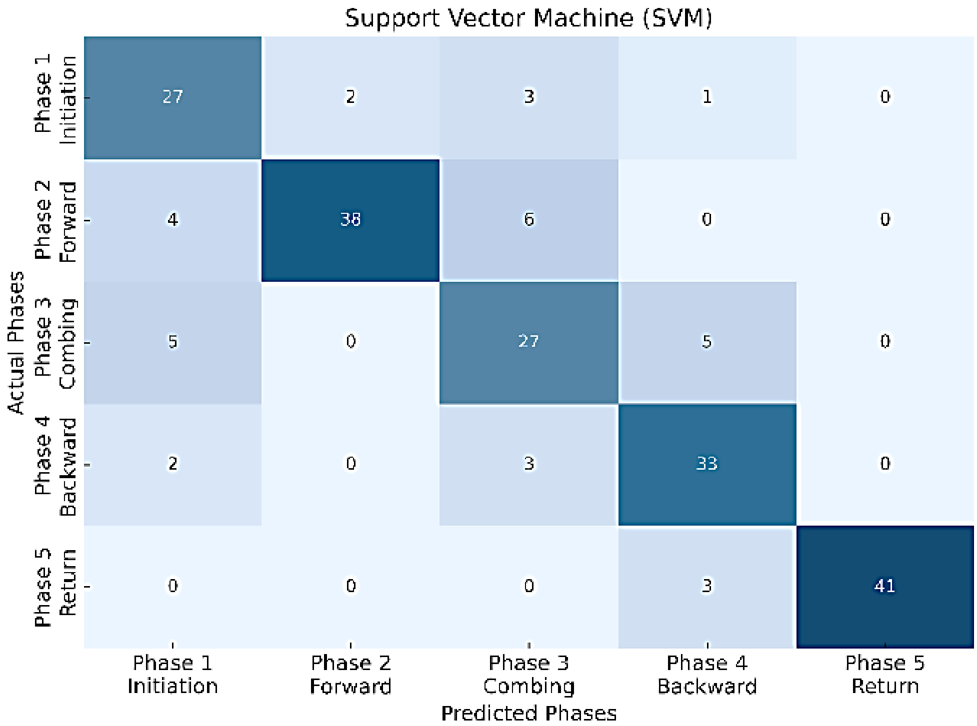

Figure 6: Confusion matrix for SVM machine learning model

Table 3: Comparison of machine learning models

Model	F1 Score	Accuracy (%)
Naïve Bayes	0.769	77.5
Support Vector Machine	0.817	83.5
Random Forest	0.758	76.6
k-Nearest Neighbour	0.685	70.0

4. Conclusion

This study demonstrated the feasibility of classifying functional upper limb movement phases during the IHC activity through the integration of sEMG, joint kinematic analysis and supervised machine learning. The use of time-domain EMG features enabled accurate characterization of muscle activation patterns associated with phase-specific motor tasks. Joint angle analysis revealed consistent kinematic signatures across the shoulder, elbow and wrist joints, supporting the segmentation and interpretation of functional movements. Among the classification models evaluated, the SVM achieved the highest performance. This underscores the potential of SVM in distinguishing subtle neuromuscular transitions across movement phases, particularly in applications where precision is essential. The integration of EMG and motion capture data provides a robust framework for movement phase recognition. This combined approach holds a promising implication for real-time rehabilitation monitoring, intelligent assistive technologies and functional assessment in clinical neurorehabilitation. While the findings are encouraging, future work should address current limitations by validating the approach in larger and more diverse populations, exploring multi-session and cross-subject variability and integrating advanced machine learning techniques to enhance model adaptability and generalization. Such developments would strengthen the clinical utility and deployment readiness of EMG-based movement recognition systems in neurorehabilitation settings.

References

Akbaş A., Furmanek M.P., Hsu S., Yarossi M. & Tunik E. 2024. Perturbing reach elicits anticipatory responses in transport and grasp. *Frontiers in Human Neuroscience* **18**: 1423821.

Cai S., Chen Y., Huang S., Wu Y., Zheng H., Li X. & Xie L. 2019. SVM-based classification of sEMG signals for upper-limb self-rehabilitation training. *Frontiers in Neurorobotics* **13**: 31.

Che-Nan H. & Rambely A.S. 2022. Kinematic analysis of daily activity of touching lateral shoulder for normal subjects. *Applied Sciences* **12**(4): 2069.

Halilaj E., Rajagopal A., Fiterau M., Hicks J.L., Hastie T.J. & Delp S.L. 2018. Machine learning in human movement biomechanics: Best practices, common pitfalls, and new opportunities. *Journal of Biomechanics* **81**:1–11.

Hermens H.J., Freriks B., Disselhorst-Klug C. & Rau G. 2000. Development of recommendations for SEMG sensors and sensor placement procedures. *Journal of Electromyography and Kinesiology* **10**(5):361–374.

Kok C.L., Ho C.K., Tan F.K. & Koh Y.Y. 2024. Machine learning-based feature extraction and classification of EMG signals for intuitive prosthetic control. *Applied Sciences* **14**(13): 5784.

Mischi M. & Cardinale M. 2009. Muscle electrical activity during force modulation exercise. *Proceeding of the 4th European Conference of the International Federation for Medical and Biological Engineering,* pp. 2065–2068.

Mohd Khairuddin I., Sidek S.N., Abdul Majeed A.P.P, Mohd Razman M.A., Ahmad Puzi A., & Md Yusof H. 2021. The classification of movement intention through machine learning models: The identification of significant time-domain EMG features. *PeerJ Computer Science* **7**: e379.

Sabzevari V.R., Jafari A.H. & Boostani R. 2017. Muscle synergy extraction during arm reaching movements at different speeds. *Technology and Health Care* **25**(1): 123–136.

Schmidt M.D., Glasmachers T. & Iossifidis I. 2023. The concepts of muscle activity generation driven by upper limb kinematics. *BioMedical Engineering OnLine* **22**(1): 63.

Shilaskar S., Bhatlawande S., Chavare R., Ingale A., Joshi R. & Vaishale A. 2024. Human hand movement classification based on EMG signal using different feature extractor. *Biomedical and Pharmacology Journal* **17**(1): 71–82.

Steinhart S., Weiss P.L. & Friedman J. 2021. Proximal and distal movement patterns during a graphomotor task in typically developing children and children with handwriting problems. *Journal of NeuroEngineering and Rehabilitation* **18**(1): 178.

Tepe C. & Demir M.C. 2022. Real-time classification of EMG myo armband data using support vector machine. *IRBM* **43**(4): 300–308.

Tsai A.C., Hsieh T.H., Luh J.J. & Lin T.T. 2014. A comparison of upper-limb motion pattern recognition using EMG signals during dynamic and isometric muscle contractions. *Biomedical Signal Processing and Control* **11**: 17–26.

Yamazaki Y., Suzuki M., Ohkuwa T. & Itoh H. 2003. Coactivation in arm and shoulder muscles during voluntary fixation of a single joint. *Brain Research Bulletin* **59**(6): 439–446.

Zhang L., Jiao Z., Li Y. & Chang Y. 2025. Movement recognition and muscle force estimation of wrist based on electromyographic signals of forearm. *Biosensors* **15**(4): 259.

Department of Mathematical Sciences
Faculty of Science and Technology
Universiti Kebangsaan Malaysia
43600 UKM Bangi
Selangor, MALAYSIA
E-mail: asr@ukm.edu.my, abubakar1110@gmail.com, elyasanusi@gmail.com*

Faculty of Computing and Multimedia
Universiti Poly-Tech Malaysia
Jalan 6/91, Taman Shamelin Perkasa
56100 Wilayah Persekutuan
Kuala Lumpur, MALAYSIA
E-mail: hasyatun@uptm.edu.my

Received: 1 July 2025
Accepted: 19 February 2026

*Corresponding author